Physicochemical Surface Properties of Fe, Co, Ni, and Cu-Doped Monolithic Organic Aerogels

C. Moreno-Castilla,* F. J. Maldonado-Hódar, and A. F. Pérez-Cadenas

Deparatamento de Química Inorgánica, Facultad de Ciencias, Universidad de Granada, 18071 Granada, Spain

Received March 28, 2003. In Final Form: May 5, 2003

Fe, Co, Ni, and Cu-doped monolithic organic aerogels were prepared by the sol−gel method through the polymerization of a resorcinol formaldehyde mixture containing the metal acetates as polymerization catalysts. The aerogels were supercritically dried with carbon dioxide, and their surface morphology and pore texture were characterized by means of scanning electron microscopy, N_2 adsorption at −196 °C, and mercury porosimetry. The dispersion, distribution, and chemical nature of the metal-containing phase were analyzed by X-ray diffraction, backscattering electron imaging, energy-dispersive X-ray, high-resolution transmission electron microscopy, and X-ray photoelectron spectroscopy. According to these analyses, the surface morphology and pore texture were influenced by the metal acetate present because of its different catalytic activity and pH of the initial mixtures. The metal-containing phase was very highly dispersed in Co and Ni-doped monolithic organic aerogels, and it was homogeneously distributed in Fe and Cu-doped monolithic organic aerogels although not so highly dispersed. XPS studies provided experimental evidence of the chelation of iron and cobalt ions by the phenolic groups of the polymeric matrix but no clear evidence of the chelation of nickel and copper ions.

Introduction

Organic aerogels can be prepared by sol−gel polycondensation of certain organic monomers following Pekala's method.[1−3] Monolithic carbon or activated carbon aerogels can be obtained from these by carbonization and activation. Because of their very special properties, including high homogeneity, purity, porosity, high surface area, and electrical conductivity, carbon aerogels are promising materials for applications in the preparation of electrodes, batteries, supercapacitors, adsorbents, molecular sieves, and catalysts.[1−8]

A potentially important feature of these materials is that metal-doped monolithic carbon aerogels can be easily prepared by adding a soluble metal salt to the initial mixture.[9−21] After gelation, the metal salt is trapped within the gel structure and the metal ions can be chelated by the functional groups of the polymer matrix.[20,21] After carbonization of this aerogel to obtain the corresponding carbon aerogel, the metal-containing phase is distributed through the porosity of the carbon phase. In addition, the metal salts added can catalyze to a varying degree the polymerization or gelation process, which in turn can affect the morphology and pore texture of the organic aerogel.

It is expected that the homogeneity of the dispersion and distribution of the metal-containing phase in the final monolithic carbon aerogel, and its pore texture and morphology, greatly depends on the properties of the organic aerogel, the first solid obtained in this process. Therefore, the present study was designed to determine the physicochemical surface properties of Fe, Co, Ni, and Cu-doped monolithic organic aerogels to be used as catalysts in different reactions after their carbonization. For this purpose, the aerogels were studied by N_2 adsorption at −196 °C, mercury porosimetry, X-ray diffraction, scanning electron microscopy, high-resolution transmission electron microscopy, and X-ray photoelectron spectroscopy.

Experimental Section

Preparation of the monolithic aerogel was carried out by dissolving resorcinol (R) and formaldehyde (F) in water (W) and using Fe, Co, Ni, or Cu acetates as catalyst precursors. The stoichiometric R/F and R/W molar ratios were 0.5 and 0.13, respectively. The amount of acetate added was 1 wt % of the metal in the initial solution. Another aerogel, to be used as blank, was prepared in the same way but without adding any metal compound. The mixtures were stirred to obtain homogeneous solutions that were cast into glass molds (25-cm length × 0.5-cm

* Corresponding author. Tel.: +34-958-243-323; fax: +34-958-248-526; e-mail: cmoreno@ugr.es.

(1) Pekala, R. W. *J. Mater. Sci.* **1989**, *24*, 3221.
(2) Pekala, R. W.; Alviso, C. T. *Mater. Res. Soc. Symp. Proc.* **1992**, *270*, 3.
(3) Pekala, R. W.; Schaefer, D. W. *Macromolecules* **1993**, *26*, 5487.
(4) Pröbstle, H.; Schmitt, C.; Fricke, J. *J. Power Sources* **2002**, *105*, 189.
(5) Glora, M.; Wiener, M.; Petricevic, R.; Pröbstle, H.; Fricke, J. *J. Non-Crsyt. Solids* **2001**, *285*, 283.
(6) Petricevic, R.; Glora, M.; Fricke, J. *Carbon* **2001**, *39*, 857.
(7) Yamamoto, T.; Sugimoto, T.; Suzuki, T.; Mukai, S. R.; Tamon, H. *Carbon* **2002**, *40*, 1345.
(8) Hanzawa, Y.; Hatori, H.; Yoshizawa, N.; Yamada, Y. *Carbon* **2002**, *40*, 575.
(9) Maldonado-Hódar, F. J.; Ferro-García, M. A.; Rivera-Utrilla, J.; Moreno-Castilla, C. *Carbon* **1999**, *37*, 1199.
(10) Moreno-Castilla, C.; Maldonado-Hódar, F. J.; Rivera-Utrilla, J.; Rodríguez-Castellón, E. *Appl. Catal.* **1999**, *183*, 345.
(11) Bekyarova, E.; Kaneko, K. *Langmuir* **1999**, *15*, 7119.
(12) Lin, C.; Ritter, J. A.; Popov, B. N. *J. Electrochem. Soc.* **1999**, *156*, 3155.
(13) Miller, J. M.; Dunn, B. *Langmuir* **1999**, *15*, 7.
(14) Bekyarova, E.; Kaneko, K. *Adv. Mater.* **2000**, *12* (21), 1625.
(15) Maldonado-Hódar, F. J.; Moreno-Castilla, C.; Rivera-Utrilla, J.; Ferro-García, M. A. *Stud. Surf. Sci. Catal.* **2000**, *130B*, 1007.
(16) Maldonado-Hódar, F. J.; Moreno-Castilla, C.; Rivera-Utrilla, J.; Hanzawa, Y.; Yamada, Y. *Langmuir* **2000**, *16*(9), 4367.
(17) Maldonado-Hódar, F. J.; Moreno-Castilla, C.; Rivera-Utrilla, J. *Appl. Catal.* **2000**, *203*, 151.
(18) Moreno-Castilla, C.; Maldonado-Hódar, F. J. *Phys. Chem. Chem. Phys.* **2000**, *2*, 4818.
(19) Moreno-Castilla, C.; Maldonado-Hódar, F. J.; Carrasco-Marín, F.; Rodríguez-Castellón, E. *Langmuir* **2002**, *18*, 2295.
(20) Baumann, T. F.; Satcher, J. H., Jr.; Yoshizawa, N.; Fu, R.; Dresselhaus, M. S. *Langmuir*, **2002**, *18*(18), 7073.
(21) Fu, R.; Yoshizawa, N.; Dresselhaus, M. S. *Langmuir* **2002**, *18*(18), 10100.

10.1021/la034536k CCC: $25.00
Published on Web 06/11/2003

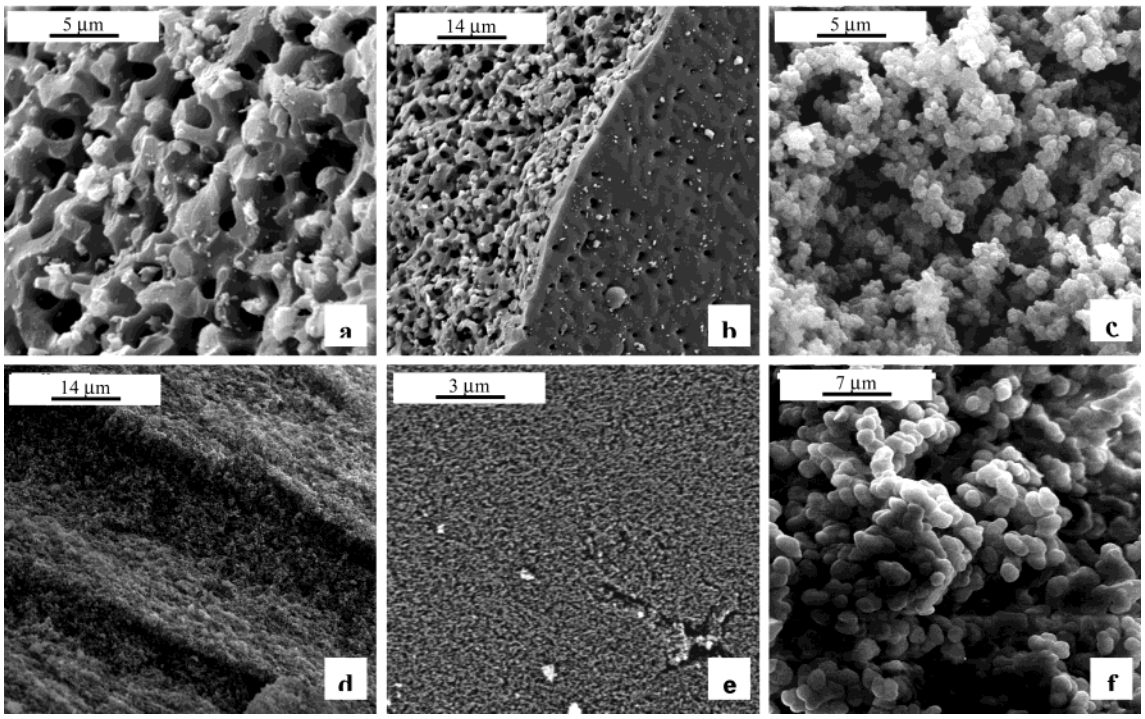

Figure 1. SEM microphotographs of A (a, b), AFe (c), ACo (d), ANi (e), and ACu (f).

internal diameter) and cured for a certain period of time. The cure cycle included 1 day at room temperature, 1 day at 50 °C, and 5 days at 80 °C. The gel rods were then cut into 5-mm pellets and supercritically dried with carbon dioxide to form the corresponding aerogels. For this purpose, the pellets were introduced in acetone for 48 h to remove the water from the pores. After that, the pellets were treated with carbon dioxide at a temperature and pressure slightly above the critical point of carbon dioxide (T_c = 31 °C, P_c = 7.4 MPa) using a CPD7501 critical point drying apparatus. Then, the liquid carbon dioxide was slowly removed, repeating the cycle several times. Samples will be referred to in the text as A followed by the metal present. Total metal content of the aerogels was obtained by burning off the aerogel at 800 °C in air and weighing the residue.

Characterization of the aerogels was carried out by the following methods: N_2 adsorption at −196 °C, for the BET surface area calculation; mercury porosimetry; X-ray diffraction (XRD); scanning electron microscopy (SEM); high-resolution transmission electron microscopy (HRTEM); and X-ray photoelectron spectroscopy (XPS).

Mercury porosimetry was obtained up to a pressure of 4200 kg cm^{-2} using Quantachrome Autoscan 60 equipment. With this technique, the following parameters were obtained: pore size distribution, PSD, of pores with a diameter greater than 3.7 nm; surface area of these pores, which will be referred to as external surface area, S_{ext}; pore volume corresponding to pores with a diameter between 3.7 and 50 nm, V_2, referred to as mesopore volume, note that mesopore volume range is classically defined as 2−50 nm;[22] pore volume of pores with a diameter greater than 50 nm, or macropore volume, V_3; and particle density, ρ.

XRD patterns were recorded with a Phillips PW1710 diffractometer using CuKα radiation. JCPDS files were searched to assign the different diffraction peaks observed. SEM experiments were carried out with a ZEISS DSM 950 (30 kV) microscope, equipped with secondary electron detector, backscattering electron detector, and using the Link Isis energy-dispersive X-ray (EDX) microanalysis system. HRTEM was carried out with a Phillips CM-20 electron microscope. Magnification was up to 600 000×, and maximum resolution was 0.27 nm between points and 0.14 nm between lines.

XPS measurements were made with an Escalab 200R system (VG Scientific Co.) equipped with MgKα X-ray source ($h\nu$ = 1253.6 eV) and hemispherical electron analyzer. Prior to the analysis, the aerogels were evacuated at high vacuum and then introduced into the analysis chamber. A base pressure of 10^{-9} mbar was maintained during data acquisition. Survey and multiregion spectra were recorded at C_{1S}, O_{1S}, and M_{2P} photoelectron peaks. Each spectral region of photoelectron interest was scanned several times to obtain good signal-to-noise ratios. The spectra obtained after background signal correction were fitted to Lorentzian and Gaussian curves to obtain the number of components, the position of the peak, and the peak areas.

Results and Discussion

SEM images of the surface morphology of sample A are depicted in Figure 1a and 1b. The polymerization of resorcinol with formaldehyde without catalyst leads to a very open structure where individual and spherical particles cannot be distinguished, as previously reported.[23−26] Thus, a continuous and highly cross-linked network was observed in the aerogel. In addition, the external surface of the pellet (Figure 1b) was observed to be less porous than the inner surface, that is, the porous pellet core was covered by a less porous surface of approximately 1-μm thick that was formed in contact with the glass mold.

The surface morphology of Fe, Co, Ni, and Cu-containing aerogels is shown in Figure 1c−1f, respectively. They were composed of fused microbead particles, and the particle size was strongly influenced by the nature of the metal. The largest particles, with diameter of about 2.5 μm, were found in sample ACu, whereas the particle size of ACo and ANi was so small that it could not be determined at the microscope resolution available. The mean particle size of sample AFe was about 0.6 μm, that is, 4- to 5-fold smaller than that of ACu but significantly greater than

(22) Bansal, R. C.; Donnet, J. B.; Stoeckli, F. *Active Carbon*; Dekker: New York, 1998.

(23) Reynolds, G. A. M.; Fung, A. W. P.; Wang, Z. H.; Dresselhauss, M. S.; Pekala, R. W. *J. Non-Cryst. Solids* **1995**, *188*, 27.

(24) Tamon, H.; Ishizaka, H.; Araki, T.; Okazaki, M. *Carbon* **1998**, *36*(9), 1257.

(25) Tamon, H.; Ishizaka, H.; Mikami, M.; Okazaki, M. *Carbon* **1997,** *35*(6), 791.

(26) Ruben, G. C.; Pekala, R. W.; Tillotson, T. M.; Hrubesh, L. W. *J. Mater. Sci.* **1992**, *27*, 4341.

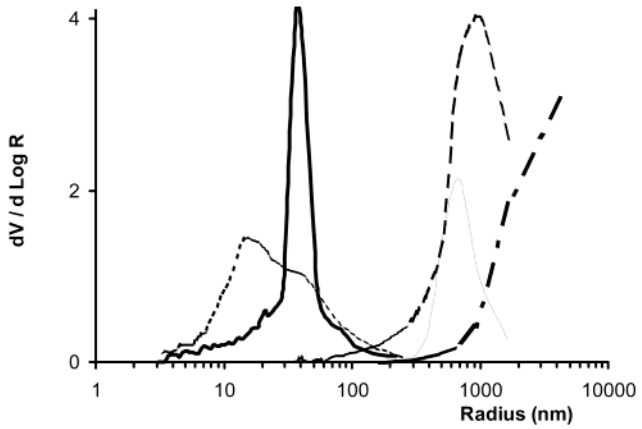

Figure 2. Pore size distribution from mercury porosimetry. A (—), AFe (– – –), ACo (—), ANi (···), ACu (– · –).

Table 1. Textural Characteristics of the Metal-Doped Monolithic Organic Aerogels

sample	ρ g cm^{-3}	V_2 cm^3 g^{-1}	V_3 cm^3 g^{-1}	S_{ext} m^2 g^{-1}	S_{BET} m^2 g^{-1}
A	0.49	0.000	0.695	4	12
AFe	0.39	0.000	1.956	6	19
ACo	0.58	0.217	0.929	88	219
ANi	0.62	0.647	0.607	128	284
ACu	0.49	0.000	1.508	2	2

that of ACo or ANi. Individual microbead particles tended to overlap, probably because of coalescence in the sol—gel state. Variations found in the size of the gel microparticles could be related to the time needed for gelation or polymerization. Thus, the larger the microparticles, the slower was the gelation process.

Textural characteristics of the aerogels are compiled in Table 1. Sample A was a macroporous material, without mesoporosity. Both external and BET surface areas were very low. The presence of metals increased the total porosity of the aerogel with respect to the blank. AFe and ACu aerogels had no mesoporosity, as in the case of sample A, but they had a larger macropore volume. In both cases, the external and BET surface areas were also very low.

Conversely, the mesoporosity of ACo and ANi aerogels increased during their polymerization, and ANi was the aerogel with largest mesopore volume. This greater mesoporosity increased the external surface area. In addition, the BET surface area of ANi and ACo was much higher than their external surface area, indicating the development of some microporosity in these samples.

PSDs from mercury porosimetry are shown in Figure 2. ACu had the widest macropores, and their volume progressively increased with increasing size. The PSDs of samples A and AFe presented their maxima at a radius of 700 and 1000 nm, respectively. The narrowest PSD corresponded to sample ACo, which had a mean pore size of 40-nm radius. The PSD of ANi presented its maximum in the mesopore region, at a radius of about 10—11 nm.

The textural properties can be related to the size of the aerogel microparticles shown in Figure 1a—1f. Thus, the smaller microparticles present in ACo and ANi give rise to a pore network containing both meso and macropores, whereas the samples with larger microparticles, such as AFe and ACu, only showed macropores. Because ACo and ANi aerogels were formed by the smallest microparticles, they exhibited the highest particle density because of the denser formation of the cross-linked microparticles.

These results clearly show that the morphology and pore texture of the aerogel depended on the nature of the metal salt, which affected the rate of the polymerization

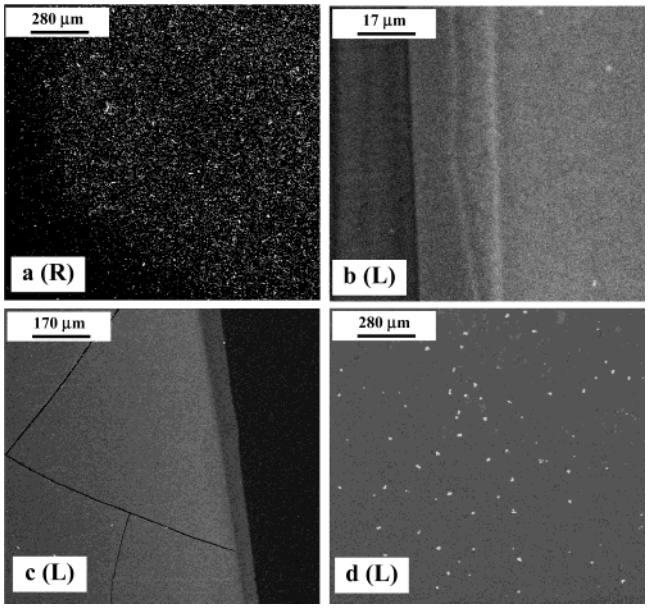

Figure 3. Backscattering electron microphotographs of radial (R) and longitudinal (L) sections of samples AFe (a), ACo (b), ANi (c), and ACu (d).

that led to the formation of the aerogel. Thus, it has been shown[27] that the concentration and acid—base character of the catalyst, among other factors, have a major influence on the surface properties of aerogels prepared from resorcinol—formaldehyde mixtures. In our case, the pH of the initial mixtures that yielded ACo and ANi aerogels was 6.4 and 6.3, respectively. This pH reached a value of 4.3, 5.4, and 4.9 for the mixtures that yielded A, AFe, and ACu, respectively. These differences in the pH of the initial mixtures may explain the distinct surface morphologies and textural characteristics of the aerogels obtained. Thus, ACo and ANi had a similar initial pH and presented a comparable surface morphology and pore texture; the gel microparticles were very small and the aerogels showed a more developed mesoporosity and greater surface area. These surface properties were different in aerogels with lower initial pHs, such as AFe and ACu, which presented larger microbead particles and developed only macroporosity. The above results indicate that cobalt and nickel acetates were better polymerization catalysts compared with the other acetates.

XRD analysis of the aerogel samples showed diffraction peaks corresponding to Fe_2O_3 in the X-ray diffraction pattern of the AFe aerogel. However, no diffraction peaks corresponding to the metal-containing phase were found in any other sample, indicating that it remained amorphous or with a particle size smaller than 4 nm.

The homogeneity of the distribution of the metal-containing phase in the pellet was studied by backscattering electrons in the SEM equipment. This produced a "chemical" image because the brightness of the image is a function of the atomic number of the element. The interpretation was simple in this case because only one metal was present in each sample. The pellets were introduced into a resin, cut in radial (R) and longitudinal (L) directions, and polished to avoid the effect of sample topography. Typical microphotographs of the metal-doped organic aerogels are shown in Figure 3a—3d.Fe and Cu-containing areas were detected at very low magnification and were uniformly distributed throughout the pellets. EDX analysis of the surface of these aerogels (Figure 4)

(27) Al-Muhtaseb, S. A.; Ritter, J. A. *Adv. Mater.* **2003**, *15*, 101.

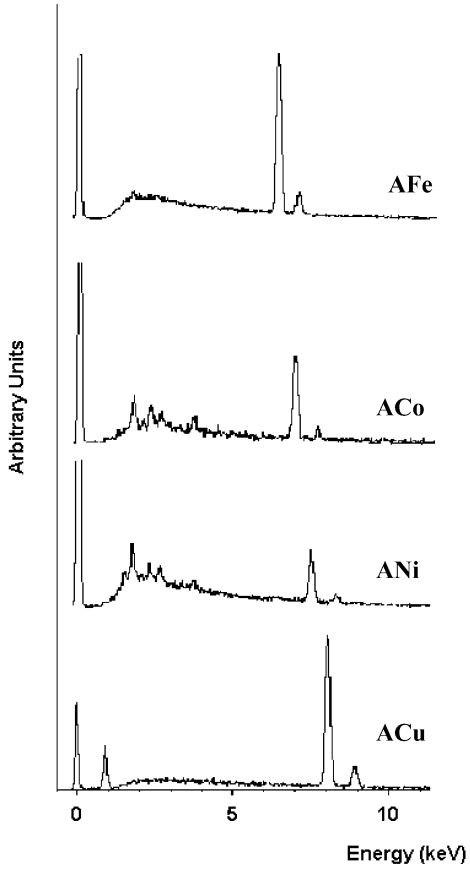

Figure 4. EDX analyses from the different metal-doped monolithic organic aerogels.

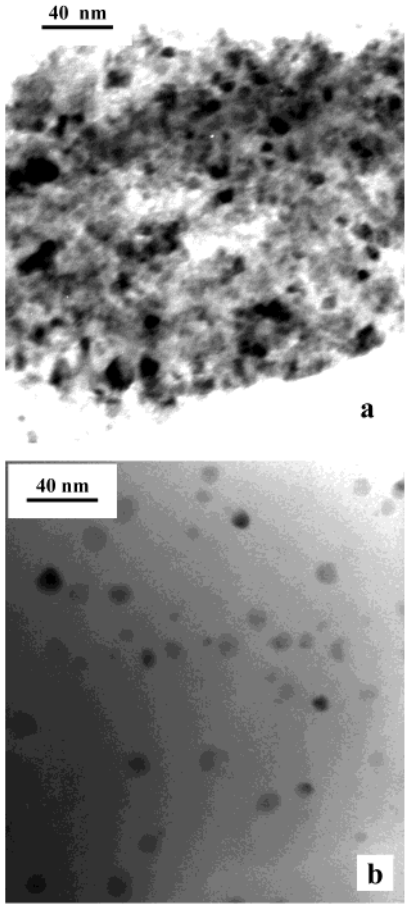

Figure 5. High-resolution transmission electron microscopy of samples AFe (a) and ACu (b).

showed the presence of both metals in their respective aerogels. The least dispersed metal-containing phase was found in the ACu aerogel, which showed the largest bright areas. Co and Ni were not detected under the same conditions, despite the fact that EDX analysis of their respective aerogels (Figure 4) showed the presence of these metals. In the ACo aerogel, some cracks were produced in the pellet during preparation of the sample for SEM observation.

HRTEM analysis showed that metal-containing particles were homogeneously dispersed at the nanometer scale in AFe and ACu aerogels (Figure 5a and 5b). However, no particles were found in the ACo and ANi aerogels, indicating that the metal-containing phase was very highly dispersed.

High-resolution XPS of the different aerogels was carried out, recording the C_{1s}, O_{1s}, and metal 2p core-level spectra. High-resolution XPS patterns corresponding to the O_{1s} region are depicted in Figure 6. The peak at a binding energy (BE) of 284.9 eV, obtained for the C_{1s} signal, was chosen as reference to carry out the deconvolution of all the spectra.

The XPS pattern of the O_{1s} region was decomposed in two components with BE values of 531.8 and 533.2 eV, assigned to C═O from ketones or carboxylic acid and single C−O bonds from alcohol, phenol, ether, or carboxylic acid, respectively.[28,29] Water appears at higher BE values of 535−536 eV. Table 2 exhibits the peak areas corresponding to these components and the O/C surface atomic ratios. The O_{1s} region in the A sample practically (98%) corresponded to single C−O bonds (533.2 eV). This is because after gelation, the polymer matrix has phenol, alcohol, and ether functionalities.

When the metals were present in the aerogels, there was a large increase in the intensity of the lower energy peak at BE of 531.1 eV, which in addition was shifted 1 eV at higher BE. These variations can be assigned to oxygen atoms bound to the metal since it has been reported that oxygen atoms coordinated to transition-metal cations have a similar O_{1s} BE.[29−32] The O/C atomic ratio practically did not change in the metal-doped aerogels compared to the blank.

Results of the XPS studies of the metal-doped aerogels are shown in Figure 7a−7d. The surface and metal content of the aerogels (M_{XPS} and M_{Total}, respectively) and the different components of the metal 2p3/2 region are compiled in Table 3. Surface metal content decreased in the order AFe ≫ ACo ≈ ACu ≫ ANi. Thus, in AFe there was a high segregation of the metal-containing phase to the surface of the pellets. This is consistent with the results obtained by XRD. Conversely, in the other metal-doped monolithic aerogels, M_{Total} was higher than M_{XPS}, indicating a higher concentration of the metal-containing phase within the pellets. The smallest value of M_{XPS} observed in the ANi aerogel can be related to its highest mesopore volume.

(28) Desimoni, E.; Casella, G. I.; Salvi, A. M.; Cataldi, T. R. I.; Morone, A. *Carbon* **1992**, *30*(4), 527.

(29) Álvarez-Merino, M. A.; Carrasco-Marín, F.; Fierro, J. L. G.; Moreno-Castilla, C. *J. Catal.* **2000**, *192*, 363.

(30) Silva, A. R.; Freire, C.; de Castro, B.; Freitas, M. M. A.; Figueiredo, J. L. *Microporous Mesoporous Mater.* **2001**, *46*, 211.

(31) Silva, A. R.; Martins, M.; Freitas, M. M. A.; Valente, A.; Freire, C.; de Castro, B.; Figueiredo, J. L. *Microporous Mesoporous Mater.* **2002**, *55*, 275.

(32) Silva, A. R.; Freire, C.; de Castro, B.; Freitas, M. M. A.; Figueiredo, J. L. *Langmuir* **2002**, *18*, 8017.

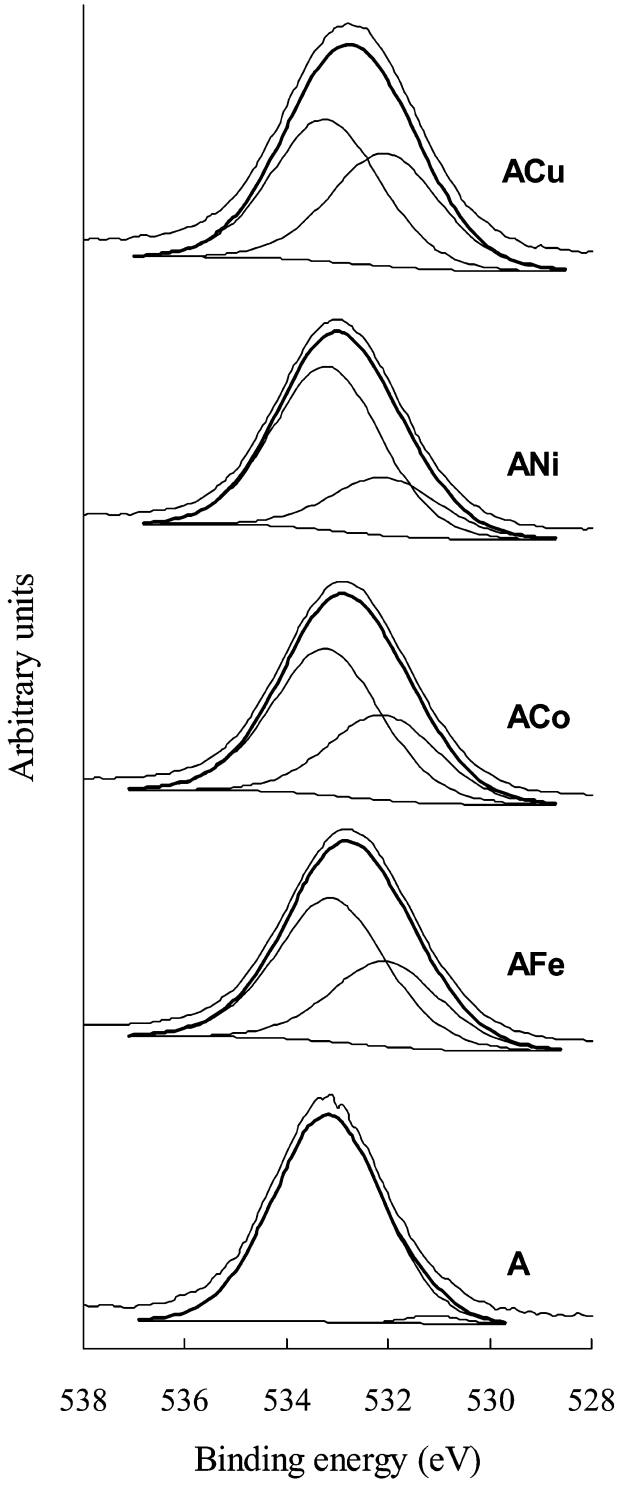

Figure 6. Curve-fitted O_{1S} core-level spectra for the different metal-doped monolithic organic aerogels and blank.

Table 2. Binding Energy Values (eV) of the O_{1S} Core-Level Spectra, Percentage of Each Peak (in Parentheses), and O/C Atomic Ratio

aerogel	C=O	C−O	(O/C) at
A	531.1 (2)	533.2 (98)	0.29
AFe	532.0 (37)	533.1 (63)	0.34
ACo	532.1 (37)	533.2 (63)	0.31
ANi	532.1 (26)	533.2 (74)	0.29
ACu	532.1 (45)	533.2 (55)	0.27

Spin−orbit splitting, multiple oxidation states, satellite structure, and adsorbent surface heterogeneity are known to complicate the analysis of the Fe_{2p} spectra.[33] The XPS

Table 3. Binding Energy Values (eV) of $M2p_{3/2}$ Components, Their Percentage (in Parentheses), and Surface (M_{XPS}) and Total (M_{Total}) Metal Contents

aerogel	$M2p_{3/2}$			% M_{XPS}	% M_{Total}
AFe	711.4 (42)	713.3 (39)	715.5 (19)	2.17	1.9
ACo	781.9 (34)	784.7 (28)	787.7 (38)	0.55	1.9
ANi	856.7 (44)	862.1 (56)		0.04	1.8
ACu	934.0 (48)	935.3 (52)		0.47	2.6

pattern of the $Fe_{2p3/2}$ region (Figure 7 a) was qualitatively very similar to that reported elsewhere.[34] The three components of the $Fe_{2p3/2}$ region found in the latter work were shifted about 1 eV to lower BE values with regard to those reported in the present work. This can be attributed, in part, to our assignation of the C_{1s} reference peak at 284.9 eV (0.4 eV higher). In addition, the truly higher BE values found in the present work (0.6 eV) may indicate smaller particle size in our AFe aerogel. This is because the neighbor atoms in a disperse system are fewer than in the bulk, and so the electrons are also fewer. The consequence is a less effective core-hole screening and the BE of the orbital shifts to higher energy.[35]

According to the above considerations, the component at 711.4 eV can be due to FeO(OH), which appears at 711.6 eV.[35] In addition, both components at 711.6 and 713.3 eV can also be assigned to Fe^{3+} oxides, reported to have BE values of between 710.7 and 712 eV.[36] The third component at 715.5 eV was assigned to iron ions complexed with electronegative surface ligands.[34] Thus, iron ions in the aerogel can be chelated by two close phenolic groups bound to the polymeric matrix.

The XPS pattern of the Co_{2p} region (Figure 7b) is also complicated by the presence of shake-up satellites together with the $Co_{2p3/2}$ and $Co_{2p1/2}$ photolines.[35−38] The first component of the $Co_{2p3/2}$ region at 781.9 eV and a typical satellite feature detected at around 787 eV suggests a Co (II) oxide/hydroxide composition.[35] The second component at 784.7 eV could be due to the chelation of the Co^{2+} ions with the phenolic groups of the polymeric matrix, as in the case of the Fe^{3+} ions.

The $Ni_{2p3/2}$ region (Figure 7c) had two components at 856.7 and 862.1 eV. The first component at 856.7 eV can be due to either $Ni(OH)_2$, which has a BE of 856.3 eV,[36] or nickel acetate, with a BE of 856.5 eV.[39] The latter compound derives from the metal precursor that was used to prepare this aerogel and was not completely decomposed. In addition, when a diamagnetic Ni(II) complex was anchored to an activated carbon through its hydroxyl groups, a peak at 856.1 eV was observed.[30] Therefore, in the ANi aerogel, the XPS data could not unambiguously determine whether nickel(II) ions were chelated by the phenolic groups of the polymeric matrix. The other component at higher BE corresponded to a satellite of the main peak characteristic of a Ni^{II}-O bond.[36]

The $Cu_{2p3/2}$ region (Figure 7d) was composed of two components at 934.0 and 935.3 eV. In copper-doped organic

(33) Li, T. C.; Seshardi, G.; Kelber, J. A. *Appl. Surf. Sci.* **1997**, *119*, 83.
(34) Pakula, M.; Biniak, S.; Swiatkowski, A. *Langmuir* **1998**, *14*, 3082.
(35) Kónya, Z.; Kiss, J.; Oszkó, A.; Siska, A.; Kiricsi, I. *Phys. Chem. Chem. Phys.* **2001**, *3*, 155.
(36) Wagner, C. D.; Riggs, W. M.; Davis, L. E.; Moulder, J. F.; Muilenberg, G. E. *Handbook of X-ray Photoelectron Spectroscopy*; Perkin-Elmer, Physical Electronics Division: Eden Prairier, MI, 1978.
(37) Gouérec, P.; Savy, M.; Riga, C. *J. Electrochim. Acta* **1998**, *43*, 743.
(38) Khassin, A. A.; Yurieva, T. M.; Kaichev, V. V.; Bukthiyarov, V. I.; Budneva, A. A.; Paukshtis, E. A.; Parmon, V. N. *J. Mol. Catal. A* **2001**, *175*, 189.
(39) http://srdata.nist.gov/xps/index.htm.

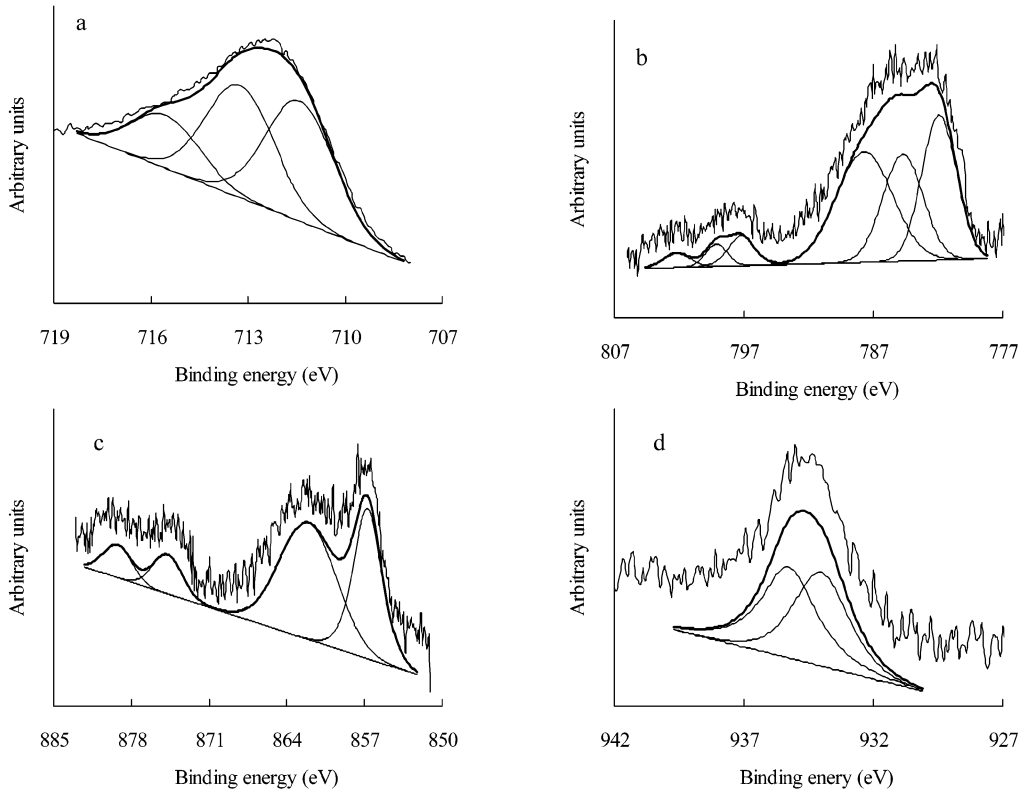

Figure 7. Curve-fitted metal $2p_{3/2}$ core-level spectra for the different metal-doped monolithic organic aerogels. AFe (a), ACo (b), ANi (c), and ACu (d).

aerogels obtained by an ion-exchange method,[21] a component at 934.5 eV was assigned by the authors to the ion-exchange copper in the aerogels. In addition, the BE of $Cu_{2p3/2}$ in copper (II) oxide[39] is 934.1 eV. Therefore, in our case the component peak at 934.0 eV is more likely due to copper oxide, although chelation with the phenolic groups of the polymer cannot be ruled out. As in the case of ANi, the XPS technique alone could not unambiguously detect the existence of copper ions bound to the polymer matrix. The second component at 935.3 eV can correspond to the copper acetate, BE value of 935.0 eV,[39,40] that was used to prepare the aerogel and that was not totally decomposed.

Conclusions

Surface morphology and pore texture of Fe, Co, Ni, and Cu-doped monolithic organic aerogels depended on the nature of the metal salt because it affected the polymerization process that led to the formation of the aerogel. Nickel and cobalt acetates, whose initial mixtures present higher pH values, seem to be better catalysts than iron or copper acetates, inducing faster reactions. Thus, Co and Ni-doped monolithic organic aerogels were formed by the smallest gel microparticles, which gave rise to a pore network containing both meso- and macropores. In addition, these aerogels had some microporosity, whereas Fe and Cu-doped monolithic organic aerogels were only macroporous solids.

The metal-containing phase could not be detected by XRD or HRTEM in Co and Ni-doped monolithic organic aerogels, indicating that it was highly dispersed. HRTEM and SEM showed that the metal-containing phase in AFe and ACu was homogeneously dispersed. According to the XPS data, some of the metal ions in AFe and ACo aerogels were chelated by the phenolic functionalities of the polymeric matrix. In contrast, this could not be unambiguously detected in the case of ANi and ACu. Moreover, in the latter aerogels, part of the metal seemed to be acetate derived from the metal salt used in the preparation of the aerogels. Finally, in the AFe aerogel there was segregation of the metal-containing phase to the external surface of the pellet. Conversely, the surface metal content in the other aerogels was smaller than the total metal content.

Acknowledgment. We acknowledge financial support from MCYT and FEDER, project MAT2001-2874.

LA034536K

(40) Wang, R. M.; Chai, C. P.; He, Y. F.; Wang, Y. P.; Li, S. B. *Eur. Polym. J.* **1999**, *35*, 2051.